Available online at www.sciencedirect.com

ScienceDirect

journal homepage: www.elsevier.com/locate/he

Effects of surface morphology changes on FTIR-ATR spectroscopy with compacted Sodium Alanate ($NaAlH_4$) during cycling

Matthias Enders [a], *Chao Zhu* [b], *Maximilian Kleber* [a], *Georg Derscheid* [a], *Rüdiger Berger* [b], *Hans-Dieter Bauer* [a,*], *Birgit Scheppat* [a]

[a] *RheinMain University of Applied Sciences, Am Brueckweg 26, D-65428 Ruesselsheim, Germany*
[b] *Max Planck Institute for Polymer Research, Ackermannweg 10, D-55128 Mainz, Germany*

HIGHLIGHTS

- Hydrogen content of $TiCl_3$-doped $NaAlH_4$ compacts was monitored via FTIR-ATR spectra.
- Changes in pellet surface morphology during cycling affect the measurements.
- Different approaches to ensure long-term signal-coupling were applied and compared.
- For samples involving gas sorption and material conversion, a small contact area improves the ATR measurement.
- Relevant for "fuel level sensors" for various metal hydride storage systems.

GRAPHICAL ABSTRACT

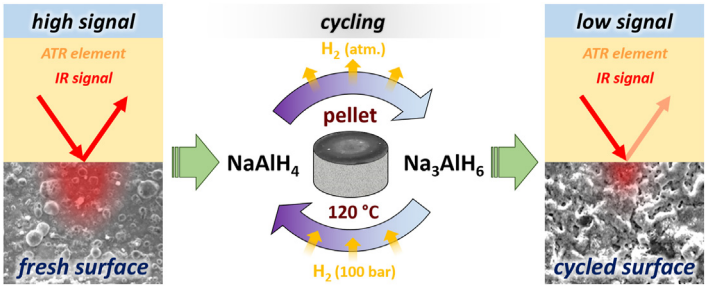

ARTICLE INFO

Article history:
Received 17 March 2022
Received in revised form
30 August 2022
Accepted 2 October 2022
Available online 21 October 2022

Keywords:
Hydrogen storage
Solid-state storage materials
Alanates

ABSTRACT

The hydrogen content during ab-/desorption of complex metal hydrides can be monitored via FTIR-ATR spectroscopy. Through cycling, the surface morphology of the pellet sample may alter due to the various material changes (e.g., granularity, volume, composition) and contribute to the spectral changes in an undesirable way.

Therefore, the desorption of the first reaction step of $TiCl_3$-doped $NaAlH_4$ compacts was investigated in terms of optical signal stability. It was found that optical signal degradation occurs with an increasing number of ab-/desorption cycles. Different hydrogen cycling procedures identified changes in temperature during cycling to further degrade the signal. Using SEM and SFM measurements, a roughening of the pellet surface was observed as an effect of cycling. For reliable optical monitoring, different approaches to ensure long-term signal-coupling have been applied and their benefits compared. Thereby, dimensional

* *Corresponding author.*
E-mail address: hans-dieter.bauer@hs-rm.de (H.-D. Bauer).
https://doi.org/10.1016/j.ijhydene.2022.10.014

Hydrogen content sensor
Optical hydrogen sensor
Spectroscopy

changes in the surface flatness were found to be the dominant factor controlling the optical signal quality.

The experimental results allow a more adequate operation of the measurement method and may be relevant for similar optical sensing applications, especially for "fuel level sensors" needed for various solid-state hydrogen storage systems.

Introduction

Hydrogen as a safe, sustainable, and efficient energy carrier is a widely anticipated option to establish a clean-energy economy in the future [1,2]. Although its gravimetric energy density is superior to that of diesel or gasoline, the volumetric storage densities that can be achieved by conventional methods of liquefaction and high-pressure storage are comparatively low [3]. In this context, solid-state storage using metal hydrides offers an opportunity to store hydrogen in an efficient and safe way at low refueling costs by increasing the volumetric hydrogen density at moderate operation pressures and temperatures [4–7].

One of the most prominent and widely investigated complex metal hydrides is sodium alanate ($NaAlH_4$) [5,8–11]. Among other potential hydrides, the material is characterized by its advantageous thermodynamics, high reversibility and easy availability of raw materials [12–14]. The hydrogen release and uptake proceed in a two-step solid-solid reaction with a combined storage density of 5.6 wt% H_2 (theoretical value):

$$3\ NaAlH_4 \rightleftharpoons Na_3AlH_6 + 2\ Al + 3H_2\ (3.7\ wt\%) \quad (1)$$

$$2\ Na_3AlH_6 \rightleftharpoons 6\ NaH + 2\ Al + 3H_2\ (1.9\ wt\%) \quad (2)$$

In order to enable the overall reaction to proceed reversibly, a dopant needs to be added to the pristine material as a catalyst. Since the catalyst is not involved in the storing process, the kinetic improvement is associated with a decrease in storage capacity. Therefore, the addition of 2–4 mol% catalyst provides a favorable balance between enhanced kinetics and remaining storage capacity [15]. In particular titanium-based dopants like $TiCl_3$ and $TiCl_4$ have been very influential among others [15–18].

Another aspect that affects the ab-/desorption process is the heat transfer from the reaction enthalpy. The thermal conductivity of powdery hydride beds is in the range of 1 $Wm^{-1}\ K^{-1}$ or even below [19]. A simple way to increase the thermal conductivity and the volumetric storage density can be found by compaction of the loose powder into pellets [20,21]. Moreover, pellets offer much easier handling, and the reactivity with oxygen or humidity is drastically reduced compared to the powdery material [22,23].

For commercial use of metal hydride storage systems, reliable and straightforward access to the used hydrogen capacity is required—the filling level. Recording the amount of stored hydrogen is challenging since the hydrogen is bound within the material and not directly measurable (volumetric methods require a prior acquisition of the amount of hydrogen added; weighing involves high accuracy due to the high backload of the tank system and needs to be insensitive against shocks). Former studies on the hydrogen desorption of $NaAlH_4$ pellets showed that the hydrogen charging level could be tracked by the change of the vibrational bands' intensities via FTIR (Fourier Transform Infrared) spectroscopy [24,25]. Due to the high absorbance of the material, the ATR (Attenuated Total Reflection) method was chosen. The method makes use of the evanescent wave that forms at the interface of a highly refractive optical element and a lower refractive sample into which the evanescent field penetrates (see Fig. 1). If there is any absorption, the evanescent wave may be absorbed to a certain degree. The remaining field is then totally reflected and carries the spectral fingerprint of the material (for more details, see Refs. [26,27]). In order to provide a reasonable optical signal, the alanate sample needs to be in tight contact with the optical element. The contact has to be kept securely throughout all hydrogen loading and unloading cycles. Even if the cycling stability of $NaAlH_4$ is reported to be excellent [28], most of the investigations on the powder and compacted samples were performed volumetrically with a Sieverts type apparatus or by thermogravimetric analysis (TGA) and were not focused on the optical behavior of the material during cycling [23,28–37].

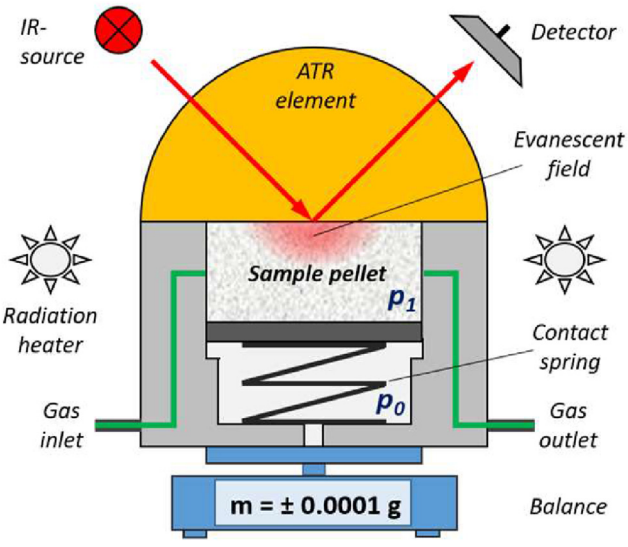

Fig. 1 – Schematic representation of the measurement setup (p_0 = ambient pressure, p_1 = sample pressure).

Thus, this work aimed to investigate the optical cycling stability of 2 mol% $TiCl_3$-doped sodium aluminum hydride compacts for long-term monitoring of the filling level. Particular emphasis was given to the surface morphology of the compacts as the contact between the interface of the $NaAlH_4$ sample and the optical ATR element represents the crucial linking point for the optical data acquisition. Also, the material was observed in terms of different cycling treatments with varying thermal process sequences and how these affect the optical signal and desorption behavior of $NaAlH_4$ compacts. Therefore, the hydrogen desorption measurements of the $NaAlH_4$ phase were performed under isothermal and isobaric conditions by FTIR-ATR-spectroscopy parallel to gravimetry to follow the solid-solid reaction from the $NaAlH_4$ (tetragonal) to the Na_3AlH_6 (monoclinic) compound.

Experimental

Material preparation

$NaAlH_4$ (hydrogen storage grade) and $TiCl_3$ dopant were used as received from *Sigma Aldrich*. The dopant was added by a dry milling process in a planetary ball mill (3 g $NaAlH_4$, 2 mol% $TiCl_3$, 20 milling balls of 10 mm diameter made of hardened steel, 1 h milling time at a rotational speed of 350 rpm with a cooling interval of 0.5 h after each 0.5 h of milling). Subsequently, the milled powder material was exposed to a hydrogen atmosphere (10 MPa, 120 °C, 2 h) to ensure a fully loaded material.

Samples were prepared by compacting 500 mg of the powder material at a pressure of 250 MPa (unless otherwise specified) into a cylindrical mold. Compaction formed a pellet (Ø = 10 mm, h ≈ 5 mm) with a smooth and visually reflective surface (substantial for a profound contact between ATR unit and sample). The material handling steps were performed in a glove box with a nitrogen atmosphere ($O_2 \leq 20$ ppm, $H_2O \leq 0.5$ ppm). For more information, refer to Ref. [38].

Measurement equipment and procedure

Parallel FTIR-ATR-spectroscopy and gravimetry

The spectroscopic and gravimetric hydrogen desorption measurements were performed with an FTIR-spectrometer "Spectrum 65" from *PerkinElmer*© and a "Cubis MSE524P-100-DU" balance from *Sartorius*© with a modified windshield. Additionally, the spectrometer was equipped with a "Seagull" reflection-accessory from *Harrick Scientific*© to measure the compacts in ATR reflection mode. Each spectroscopic measurement was taken by one single scan with a resolution of 4 cm^{-1} to maintain a fast data acquisition (<10 s). The temperature was remotely controlled by a radiative heating system installed inside the spectrometer's sample chamber.

In order to separate the sample from the surrounding atmosphere, a self-developed high-pressure ATR cuvette was used as schematically depicted in Fig. 1. The sample is pressed against the ATR unit by a contact spring to compensate volume changes of the $NaAlH_4$ material during hydrogen ab-/desorption [5]. To protect the ATR unit made of zinc selenide against solid-solid reactions and mechanical stress, a diamond platelet of 100 μm thickness is used as a separating layer between the ATR unit and sample. Due to the optics used, a slightly elliptical spot with a diameter of ≈6 mm is formed on the sample. In this way, the spectral measurement is averaged over a sufficiently large area, eliminating sample-specific deviations of local measuring points.

Prior to desorption measurements, the cuvette was pressurized with 40 MPa of nitrogen to prevent a partial hydrogen release during the preheating period to the intended temperature. After reaching the desorption temperature, the pressure was released to start the desorption process. A check valve with a backpressure of 7 kPa was used to avoid access to the surrounding atmosphere. A more detailed explanation can be found elsewhere [25,38].

The ATR cuvette was mounted into a cycling setup for an automated cycling procedure, as schematically presented in Fig. 2. Thereby, the sample pellet can remain inside the cuvette and stay in constant contact with the ATR element. A complete cycle consists of one hydrogen absorption and one desorption step (here, only for the first reaction following Eq. (1)). The parameters used for absorption were 10 MPa at 120 °C for 2 h and with the same temperature and time against a backpressure of 7 kPa for desorption. To provide a fully loaded material, hydrogen pressure was kept at 10 MPa until a temperature below 30 °C was reached after the final absorption step.

Surface morphology

Scanning force microscopy (SFM) measurements were performed in an argon-filled glove box (O_2 and H_2O < 0.1 ppm) using an "MPF-3D" from *Oxford Instruments* [39]. Sample protection was realized by means of a sealed Ar filled box to transfer samples from the FTIR-ATR system to the glove box.

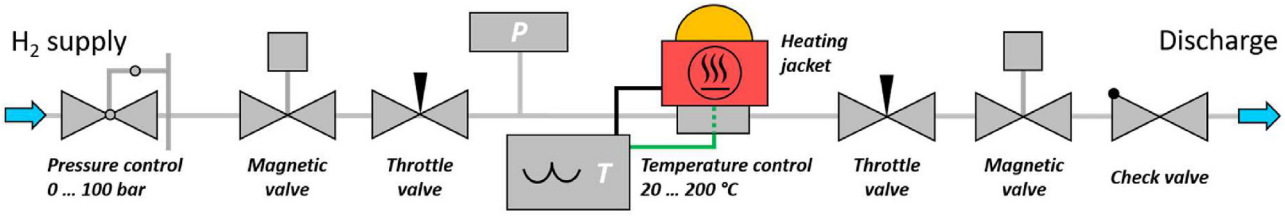

Fig. 2 – Schematic representation of the cycling setup for an automated cycling process with pressure (0–10 MPa) and temperature (20–200 °C) control. The ATR cuvette from Fig. 1 is placed inside a heating jacket (marked red) and connected to the gas piping. (For interpretation of the references to color in this figure legend, the reader is referred to the Web version of this article.)

For topography imaging, tapping mode was used (OTESPA, nominal resonance frequency 300 kHz, and nominal spring constant 26 N m^{-1}).

Scanning electron microscope (SEM) images were taken using a "JSM-6380LF" from *Jeol*. During the transfer process, the samples were briefly exposed to the atmosphere (5–10 s). Some slight surface reactions occurred, but these can be considered negligible for the qualitative comparison of the surface structure. However, if the contact with air is too long, the material's morphology can be significantly changed (cracking), even if no apparent macroscopic reaction is present [40].

Results and discussion

FTIR-ATR-spectroscopic measurements

The hydrogen desorption of sodium alanate has been measured in-situ by gravimetry parallel to FTIR-ATR spectroscopy. The spectral measurement was performed in the 600 cm^{-1} to 2200 cm^{-1} region. The most prominent vibrational bands for that region were attributed to the Al–H stretch modes of the tetrahedral $NaAlH_4$-phase (1620–1680 cm^{-1}) and of the octahedral Na_3AlH_6-phase (1250–1320 cm^{-1}) [41–44]. A more specific description can be found in Refs. [25,41]. Previous works showed that the spectral intensity changes of the Na_3AlH_6 phase correlate to the amount of released hydrogen of the gravimetrical measurement. Therefore, the purely optical signal can indicate the hydrogen filling level of the material [24,38]. It should be mentioned that the relatively significant intensity changes in the range of 1800–2000 cm^{-1} are not assigned to a specific vibrational band. The intensity changes possibly arise from the different refractive indices of the respective phases and the resulting change in reflection by the ATR method. Nevertheless, these changes are also suitable for monitoring the loading state, mainly due to the high-intensity changes between fully loaded and unloaded material.

The typical ATR spectra of the hydrogen desorption of the $NaAlH_4$ phase are shown in Fig. 3a for the first desorption cycle. The upper curve corresponds to the starting point (0 min, red) of the desorption process of a fully-loaded pellet. The lower curve (90 min, green) coincides to the end of the first

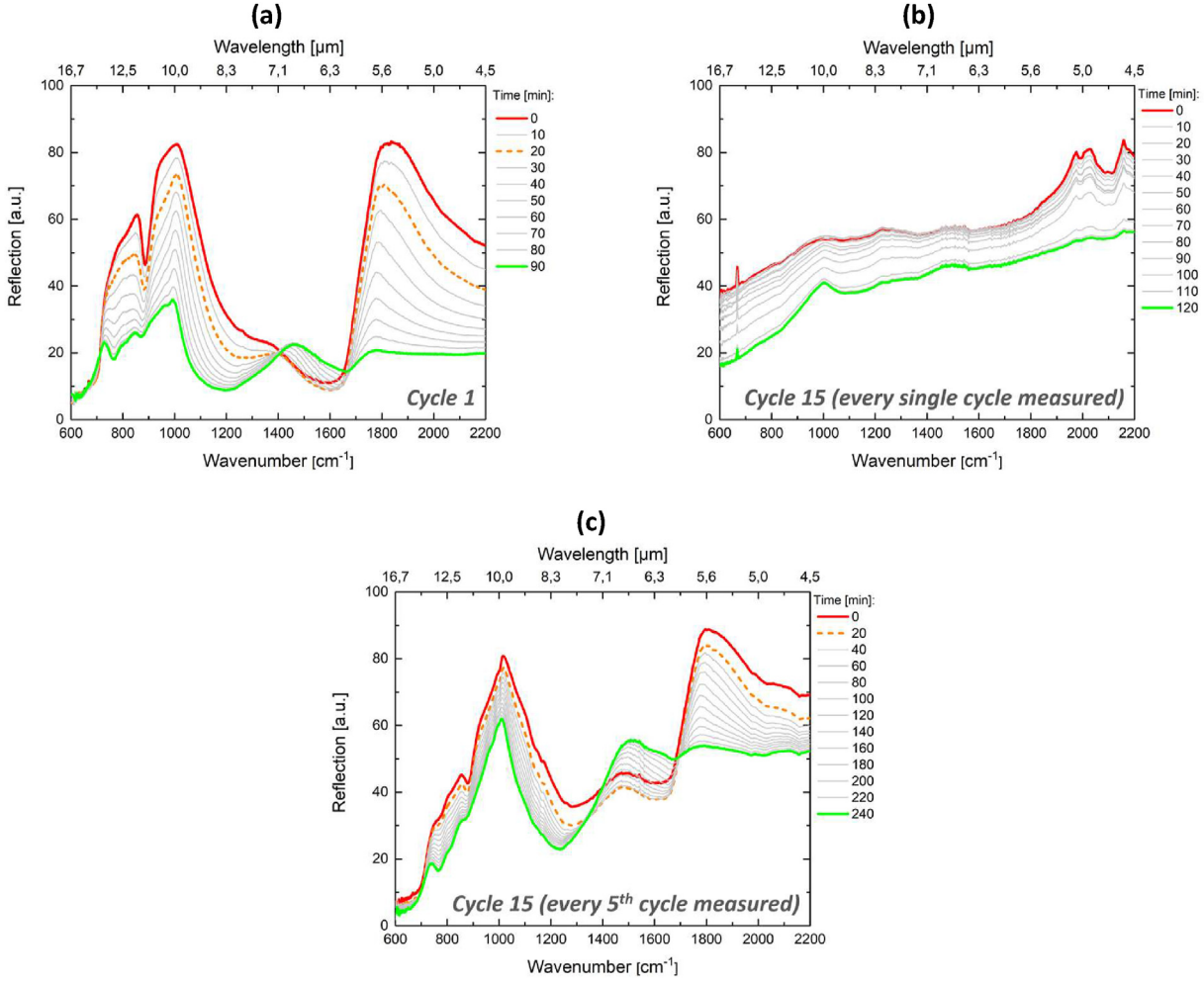

Fig. 3 – FTIR-ATR measurement of hydrogen desorption of $TiCl_3$-doped $NaAlH_4$ pellets: a) spectra for the first cycle, b) spectra for cycle 15, where each cycle was measured with the FTIR-ATR setup, and c) spectra for cycle 15, where the optical measurement was performed after every fifth cycle (cycling between the spectral measurements was performed with the cycling setup).

reaction step (Eq. (1)). During the desorption process, the upper spectrum gradually changes into the lower spectrum ($NaAlH_4$ => Na_3AlH_6), releasing a hydrogen amount of about 3 wt% (gravimetric measurement). Note that there is a slight deviation from a continuous intensity increase in the range of 1630 cm^{-1} ($NaAlH_4$) at the beginning of the desorption process until the orange curve (20 min) is reached. This can be attributed to a slightly improved contacting of the sample to the ATR element after the nitrogen backpressure has been released (for more details, see Ref. [38]).

Compared to the first cycle, significant changes in desorption characteristics can occur with increased cycling steps. The changes may result from the pulverization and aggregation of the powder grains and the formation of new diffusion pathways and gas channels. Moreover, irreversible phase separations and encapsulations may lead to a reduced storage capacity (e.g., areas of increased aluminum concentration [28]). The majority of these mechanisms take place within the first ten cycles (activation of the material towards a steady desorption behavior) [23,37].

Accompanying the changes in the desorption characteristics due to cycling, changes in the spectral measurements were also observed. These can be so extensive that the spectral phase transformation could no longer be traced, as shown in Fig. 3b (no specific absorption bands visible, only baseline shifts). As a result, purely optical measurement can no longer be used. The irregular signal quality revealed another aspect for samples with the same cycles. Samples for which each desorption was measured by the FTIR-ATR spectroscopic setup (Fig. 3b) showed a much faster optical signal degradation than those for which the optical signal was recorded at larger intervals, as demonstrated in Fig. 3c for the measurement of every fifth cycle. Hence, the intensity signal showed a quasi-dependence on the number of measurements in the FTIR-ATR setup instead of the number of material cycles. The low energy input of the infrared radiation rules out an influence of the FTIR spectrometer. A potential cause of the phenomenon is the temperature changes between the desorption runs within the FTIR-ATR setup. The cuvette, including the pellet, has to cool down to room temperature after desorption for further handling. In contrast, the cycling procedure in the cycling setup between the spectral measurements was performed at a constant temperature for the ab-/desorption steps.

Since the ATR method is based on the close contact between the ATR element and the sample, pellet images were observed before the first desorption step and after optical signal loss due to cycling, as shown in Fig. 4. The freshly compacted pellet shows a high reflectance and thus a high-quality optical surface, whereas the cycled pellet reveals a dull appearance (similar to a roughened surface). These findings are also consistent with the observations made by Lozano et al. [23] and Sulic et al. [37]. Therefore, the signal loss may be attributed to a lack of contact with the ATR crystal. The origin of this behavior may have many causes (material changes, synthesis parameters, measurement conditions). However, the signal quality is always sample-dependent and may vary from sample to sample. The primary influence is exerted by the optical surface quality and homogeneous material distribution. According to the work of Pohlmann et al. [20,45,46], optical cross-section observations for different hydride materials revealed no evident inhomogeneity for pellet diameters below 14 mm. Nonetheless, for a scaled-up pellet geometry (77 mm diameter, $NaAlH_4$), differences in packing density can occur due to inhomogeneous powder distribution within the press die and non-uniform compaction conditions as presented by Börries et al. [47].

In summary, two observations were particularly striking—on the one hand, a less reflecting appearance of the pellet surface and, on the other hand, the irregular signal quality that might be affected by the thermal treatment of the material. Therefore, a more detailed investigation of the origin of the signal loss was carried out, which is discussed in the following sections.

Effects of thermal treatment during cycling

In order to verify a temperature effect, samples were treated with 30 cycles of hydrogen ab-/desorption with different process sequences within the cycling setup. Part of the samples was cycled at a constant temperature of 120 °C, and another part with an additional cooling step and subsequent reheating to 120 °C between the individual ab-/desorption steps, as shown in Fig. 5a and b, respectively. A fast cooling to ambient temperature was realized by means of controllable fans. After cycling, the spectral measurement was

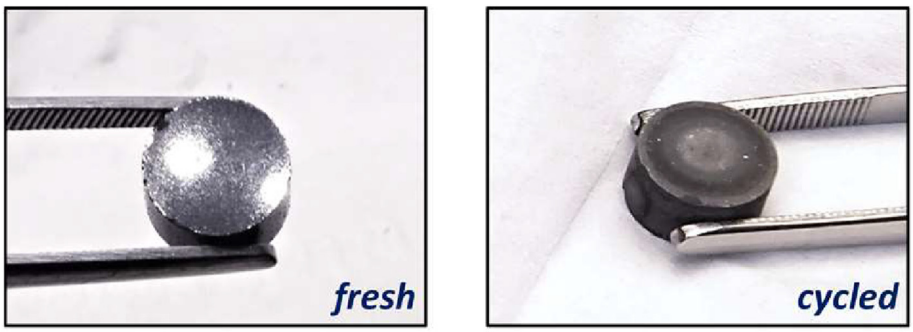

Fig. 4 – Images of a pellet before the first desorption (left) and after spectral signal loss due to cycling (right), as shown in Fig. 3.

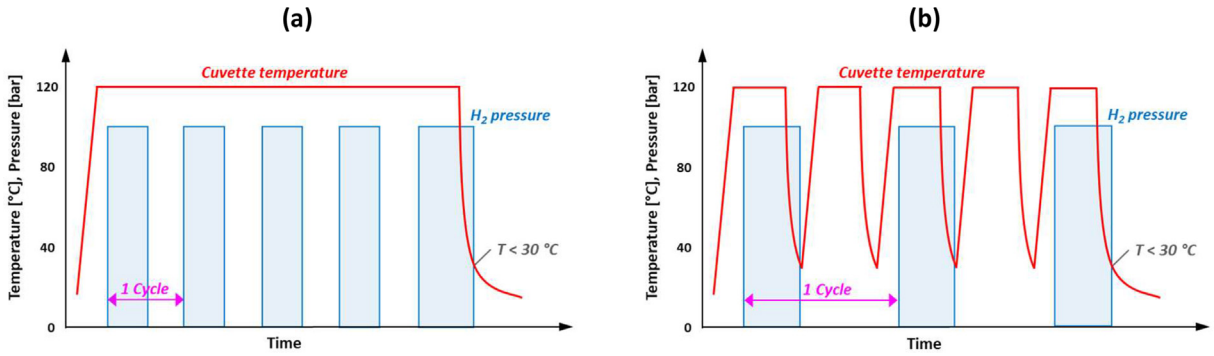

Fig. 5 – Exemplary process sequences for cycling a $NaAlH_4$ pellet inside the ATR cuvette a) without a cooling step at constant temperature and b) with an intermediate cooling step down to 30 °C between hydrogen absorption (T_{abs} = 120 °C, 10 MPa H_2, 2 h) and desorption (T_{des} = 120 °C, 7 kPa backpressure, 2 h).

performed within the FTIR-ATR setup with the procedure described previously (no further spectral measurements were taken between the cycles 1–30).

The characteristic results of the spectral measurements are presented in Fig. 6. For cycling, at a constant temperature, Fig. 6a shows the spectra of the first desorption and Fig. 6b the

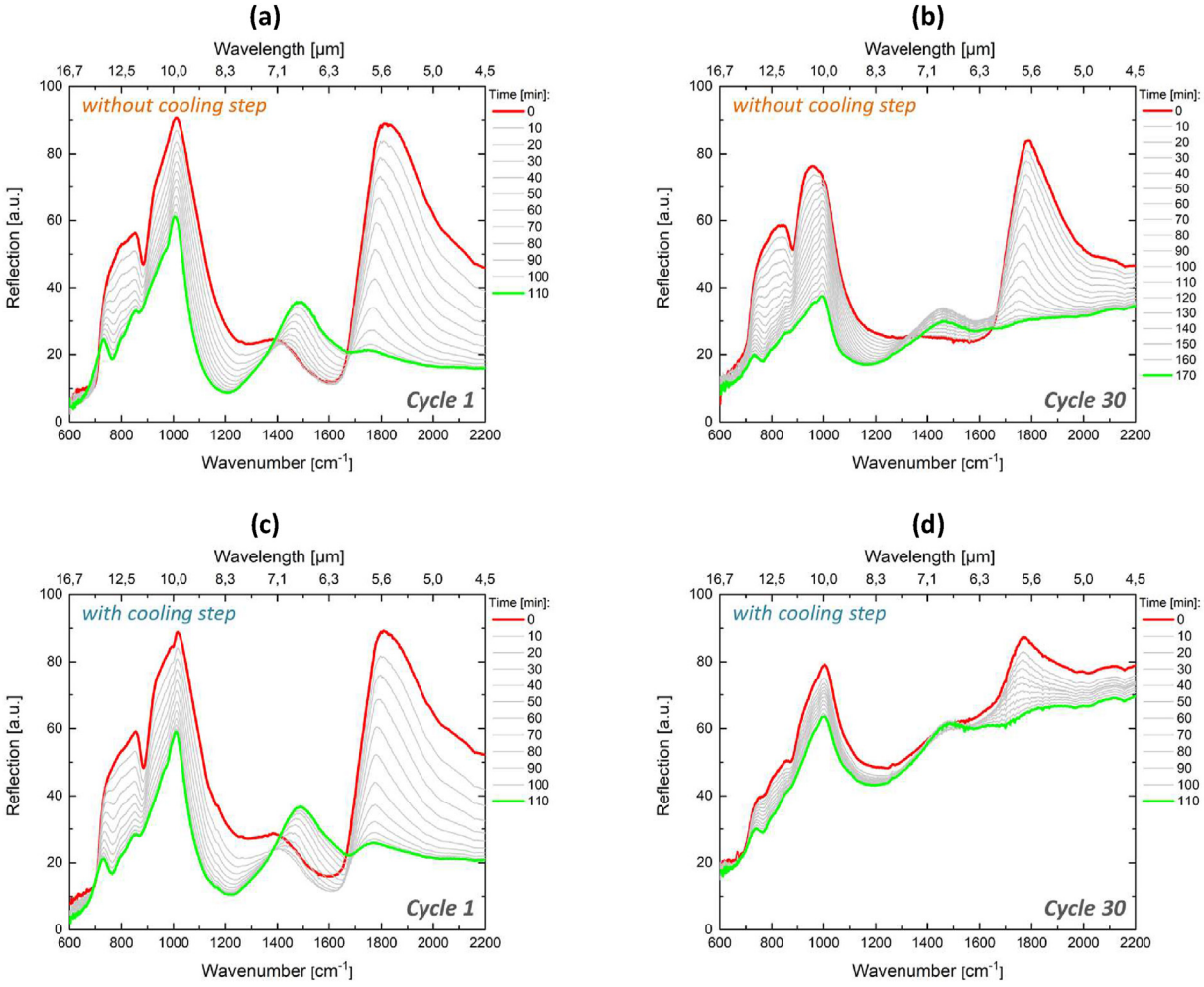

Fig. 6 – FTIR-ATR spectra of hydrogen desorption of 2 mol% $TiCl_3$-doped $NaAlH_4$ pellets at T_{Des} = 95 °C and backpressure of 7 kPa. Measurements of a) cycle 1 and b) cycle 30 for a sample with constant temperature (T_{Cyc} = 120 °C) between the individual ab/-desorption steps during cycling (cf. Fig. 2a). Measurements of c) cycle 1 and d) cycle 30 for a sample with a cooling sequence (T_{Cyc} = 30 °C.120 °C) between the individual ab-/desorption steps during cycling (cf. Fig. 2b).

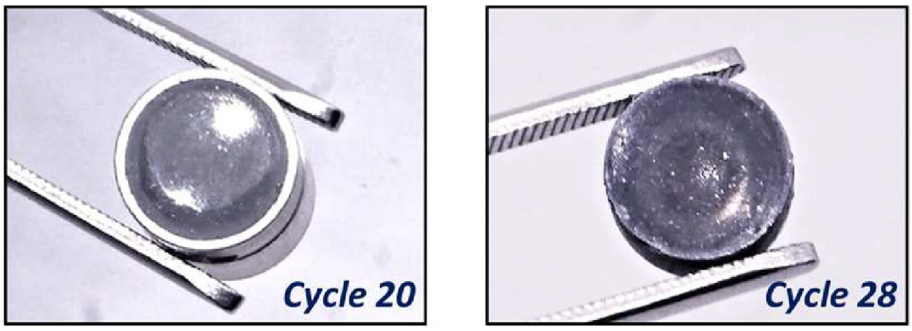

Fig. 7 – Images of 2 mol% $TiCl_3$-doped $NaAlH_4$ compacts after 20 cycles (left) and after 28 cycles (right).

corresponding spectra of cycle 30. Even after 30 cycles, the spectral intensity changes of the vibrational bands are traceable. In contrast, Fig. 6c and d show the results of the comparative spectral measurements for the first and 30th desorption in which an intermediate cooling step was performed. In this case, the spectra for cycle 30 show much weaker intensity changes during hydrogen release. The gravimetric measurement for both cases (with and without cooling step) showed hydrogen desorption of ≈2.0 wt%. Therefore, a signal deficiency due to a lack of hydrogen loading can be excluded, even if a decrease in capacity is noticeable due to cycling.

Thus, the optical signal degradation arises, at least as one potential reason, from the thermal changes between operating conditions for ab-/desorption (>100 °C) and non-operating conditions (ambient temperature) of the alanate material. It seems reasonable that the material is more stressed by the temperature changes, similar to aging. In addition, recurrent heating and cooling can cause a stronger volume contraction, which places tremendous stress on the material. Desorption kinetics also appear to be affected by the different heat treatments, as there are variations in desorption times. Van Hassel et al. [48] reported a reduction of the hydrogen storage capacity with a slower rate of hydrogen ab-/desorption after long-term exposure to 180 °C. This was explained by reduced catalytic activity, material agglomerations, and larger crystallites due to material aging. Dieterich et al. [49] investigated the cycling characteristics (>1000 cycles) of an intermetallic hydride with different cycling parameters. Thereby the material underwent different heat treatments, too. They concluded that absorption time influences hydrogen uptake toward constant capacity. Although a temperature effect was not explicitly considered, it may also be present in their work and affect hydrogen uptake.

A more detailed consideration of the effect of different temperature treatments is beyond the scope of this work and was therefore not pursued further. It is worth noting that repeated measurements yielded similar results. Although the experiments revealed a characteristic behavior, more sophisticated and comprehensive investigations on the role of temperature treatment need to be performed to provide a distinct quantitative description with respect to accuracy and reproducibility. The results of such studies may contribute to a more detailed understanding of material behavior under real operating conditions.

Surface characteristics

Since the contacting of the pellet to the ATR unit represents the linking point to the optical data acquisition, the surface was investigated by quantifying its roughness via scanning force microscopy and imaging its morphology optically, and using a scanning electron microscope.

Freshly compacted samples (e.g., Fig. 4) were used as a reference and compared to cycled pellets (Fig. 7). In order to maintain a characteristic roughness value, each sample surface was studied at five different regions with a scan size of 25 μm^2. From each scan, the root mean square (rms) roughness (R_q) and the maximum roughness depth between the highest to lowest topographic point (R_{max}) were calculated (Table 1). Since the measurements are primarily for qualitative comparison, an error analysis is not discussed further.

For the freshly pressed $NaAlH_4$ samples, a mean rms-roughness of 43 ± 6 nm for the pristine (undoped) and a slightly increased value of 62 ± 11 nm for the $TiCl_3$-doped material was found. Thus, the dopant and the doping procedure do not influence roughness to a large extent. For the sample treated with 20 cycles, a separate roughness analysis of the outer edge area and the center was performed due to the different surface reflections for those regions. The reflective inner part and dull outer region showed a deviating roughness of 86 ± 66 nm and 166 ± 55 nm, respectively. A

Table 1 – Mean surface roughness of $NaAlH_4$ pellet samples (total scan area: 5 × 25 μm^2; cf. Fig. 4 for an uncycled and Fig. 7 for the cycled samples).

Sample		Cycle	R_q [nm]	R_{max} [μm]
I. (pristine)		0	43 ± 6	0.53 ± 0.08
II. ($TiCl_3$)		0	62 ± 11	0.54 ± 0.15
III. ($TiCl_3$)	(center) (edge)	20	86 ± 66 166 ± 55	0.77 ± 0.60 1.15 ± 0.23
IV. ($TiCl_3$)		28	154 ± 71	1.09 ± 0.49

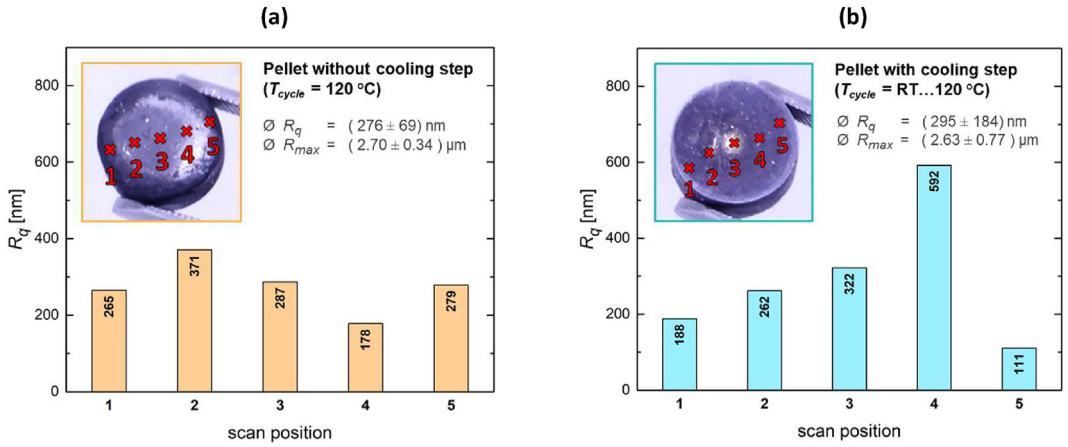

Fig. 8 – Surface roughness after 30 cycles for a pellet a) at constant temperature and b) with a cooling sequence during cycling (total scan area corresponds to 5 × 900 µm²).

similar value to the outer region was obtained for the sample treated with 28 cycles. Compared to freshly produced samples, the cycled samples exhibit an increased roughness and a significantly higher variation between the analyzed regions. The increase in roughness of cycled samples appears to be moderate. However, even small gaps will result in a significant signal loss for the ATR method. This becomes more obvious when taking the corresponding R_{max} values into account. Here, the considered cycled samples showed no or only poorly evaluable optical signals during desorption.

The surface roughness analysis was also carried out for the pellets with different tempering procedures from Fig. 6 with a scan size of 900 µm² for each region. For the pellet without a cooling step (Fig. 8a), a mean rms roughness of 276 ± 69 nm and for the pellet including a cooling step (Fig. 8b), a value of 295 ± 184 nm was measured. The R_{max} values range up to 2.70 µm. The roughness values of both samples are quite similar. In particular, the pellet which was cooled and exhibited a weak optical signal showed the highest R_q value (scan position four). However, both samples show a significantly increased surface roughness (≈280 nm) compared to a freshly compacted pellet (≈60 nm).

In addition to the surface roughness analysis, imaging methods were used for qualitative surface observation. Fig. 9 shows the microscope images of the surface of both samples with and without a cooling interval from Fig. 6. The sample without a cooling step (Fig. 9a–c) appears to be of poor optical quality since the sample with cooling (Fig. 9d–f) has a more uniform appearance. Regardless, the highly reflective areas (whitish) from Fig. 9a still indicate a good optical

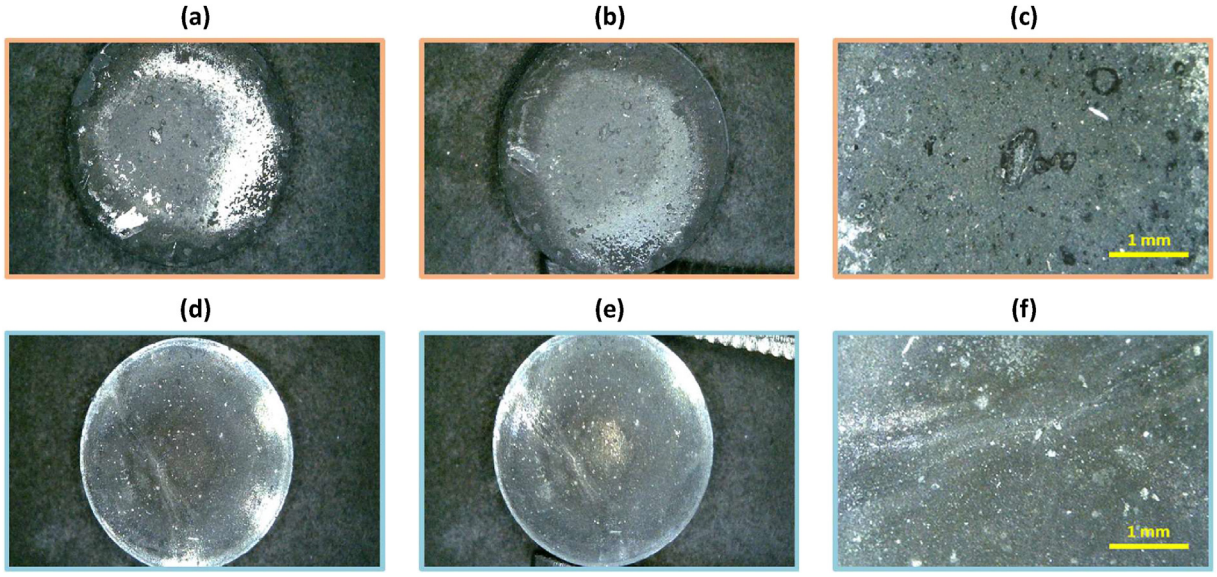

Fig. 9 – Microscope images of the surfaces of the pellet without (a–c) and with a cooling process (d–f) after cycling: a) and d) image with perpendicular light exposure, b) and e) image with a slight tilt angle of 15° to avoid direct light reflections from the exposure field, c) and f) detail view of the pellet surface.

surface quality. In contrast, the surface from Fig. 9d and e has a dull appearance, which is also apparent in the close-up image of Fig. 9f.

Supplementary to optical microscopy, different cycling conditions of pellet samples were compared by scanning electron microscopy. Fig. 10a–c shows the micrographs of a freshly compacted $NaAlH_4$ pellet, and Fig. 10d–f shows the micrographs of a pellet after 27 cycles of hydrogen ab-/desorption. For the uncycled sample, a wholly closed surface is obtained with individual protruding grains. In other words, the grains are embedded in a base layer of material. The size of the grains is mainly in the range of approx. 1–10 μm. The structure of the cycled sample resembles that of a sponge with pores (black dots) with a size of approx. 1–2 μm. The pore formation can be regarded as a result of hydrogen release during desorption.

The combined surface observations by optical microscopy, SFM, and SEM measures conclude that a surface roughening occurs by cycling. In this case, the signal deterioration results from a successively worsening contact between the sample surface and the ATR element. On the one hand, the contact loss can be ascribed to the change in porosity by simple geometrical contraction. On the other hand, the observed temperature effect for the cycling conditions may be assigned to a "kinetic surface roughening" process.

Similarly, Lozano et al. [23] observed a change in the surface structure of cycled $NaAlH_4$ compacts in which cracks and channels were formed, and Sulic et al. [37], as well as Thomas et al. [40], demonstrated pore formation. A likewise behavior with great geometrical and surface changes was also observed for compacts of other hydride materials and mixed composites [49,50].

All these findings have an increase in volume (swelling) due to cycling in common. Only a few studies considered the case of confined pellets. Continuing on from their previous research, Sulic et al. showed that $NaAlH_4$ pellets confined by aluminum tubing had a 50% less decrease in density with similar desorption characteristics to unconfined pellets [51]. Van Hassel et al. [48] showed that a pellet reinforced with an aluminum mesh increased the strength by 20–40% with reduced expansion. Concerning the current investigations, no significant volume increase of the pellets could be detected. Therefore, it is assumed that the material expansion mainly takes place in the residual porosity due to the confinement by the sample chamber of the ATR cuvette. In this case, a locally deviating swelling (even if small) can also contribute to a lack of contact, further discussed in the following section.

Measures for signal preservation of cycled $NaAlH_4$ compacts

Since the temperature changes for hydrogen ab-/desorption cannot be circumvented, or in other words, since the storage application is not permanently operated at an elevated temperature level (>100 °C), it is necessary to find thermally independent measures to maintain the optical signal quality to monitor the filling-level. Therefore, several approaches have been tested, summarized in Table 2 with the results.

While the first two approaches did not lead to any improvements in the context of the applied investigations, the latter two proved to be more instructive. Although the third approach of pre-cycling and enhanced contacting by a lowered absorption pressure stabilized the optical signal for low cycle numbers (<10), signal deterioration reappeared at higher cycles. Moreover, pressure conditions of about 10 MPa H_2 are

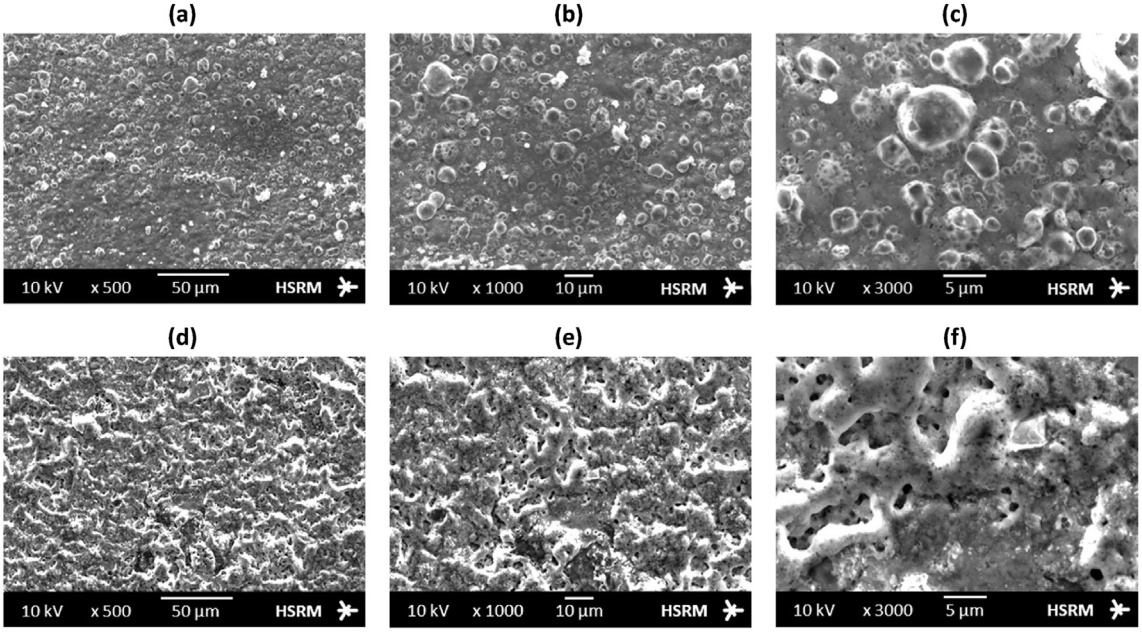

Fig. 10 – SEM images of the surface of a freshly compacted 2 mol% $TiCl_3$-doped $NaAlH_4$ pellet: a) 500×, b) 1000× and c) 3000× magnification. Surface images of a similar pellet after 27 cycles of hydrogen ab-/desorption: d) 500×, e) 1000× and f) 3000× magnification.

Table 2 – Overview of the applied approaches to maintain the optical signal's quality during cycling.

Measure	Description
I. Additives for an improved signal coupling between a sample and ATR element	Approach: Level out irregularities or pores in the sample surface with highly refractive additives – here, diamond nanopowder. Result: No improvement but deterioration of the optical signal since the admixture acted like a release agent and led to a reduced internal bonding of the material (consequence: increased surface roughening or embrittlement).
II. Increased compaction pressure during pellet production	Approach: Elevated compaction pressure (875 MPa) for the pellets' more substantial dimensional stability. Result: No improvement, since the properties of pellets with high compaction equalize to those with lower compaction in the course of cycling (see also [23]).
III. Pre-cycling of the material and adjusting the process parameters	Approach: First, increasing the contact between pellet and ATR element by a reduced H_2 pressure during absorption (p_1 => from 10 MPa to 7 MPa => higher contact force from spring, cf. Fig. 1). Second, reducing the effect of material transformations by pre-cycled pellets (10 cycles, then re-ground and re-compacted). Result: Spectral intensity changes can remain accessible for small numbers of cycles (<10), but further degradation became apparent at higher cycle numbers.
IV. Surface smoothing of cycled samples through re-compaction	Approach: Re-compaction of cycled pellets with a guiding device. Result: The smoothed surfaces showed a comparable appearance to freshly produced pellets with well-reflecting surfaces (also a closed surface with comparable roughness of ≈70 nm). However, the surface became wavy, not allowing sufficient contacting with the ATR element.
V. Adjustment of the pellet geometry	Approach: First, forming a thin pellet (<1 mm) less resistant to bending and can contact the ATR element more tightly. Second, reducing the pellet diameter to enlarge the contact pressure to the ATR element and decrease the influence of waviness due to a smaller surface area. Result: Handling of the pressing device did not allow uniform powder distribution for thin pellets, which led to wedge-shaped geometries and poor contacting. Smaller pellets showed a more stable signal quality.

still required for fast hydrogenation kinetics. At this point, it should be clarified that the contact pressure is already at a high level and is limited to a range that the optics can withstand (also, wear and tear appeared on the cuvette, and some diamond platelets fractured under the load).

A guiding device was used to reinsert cycled pellets into the press die for surface smoothing by re-compaction. The pressure required was 375–500 MPa, which exceeds the contact pressures of the ATR cuvette many times (≈7.4 MPa) and the pressure initially used for compaction (250 MPa). The smoothed surfaces showed a similar appearance to freshly produced pellets, as presented in Fig. 11. In addition, the surface roughness was measured via SFM in a similar procedure to those of section Surface characteristics with five measuring points along a line. Table 3 shows the results with an rms roughness of about 80 nm, approximately in the same range as a freshly prepared sample of about 60 nm. Moreover, the maximum roughness depths of about 1 μm are well below those of cycled samples with ≈2.7 μm after 30 cycles. For better comparability, a sample was also observed by SEM after

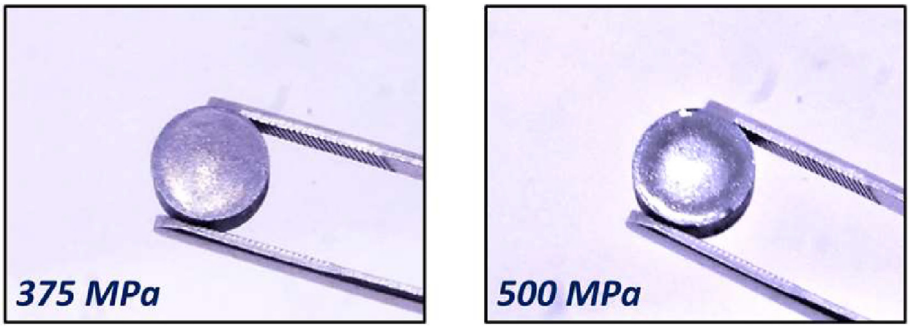

Fig. 11 – Surface images of cycled $TiCl_3$-doped $NaAlH_4$ pellets re-pressed with 375 MPa (left) and 500 MPa (right) of compaction pressure.

Table 3 – Mean values of surface roughness measurement of re-pressed pellets from Fig. 11 (total scan area: 5 × 900 μm²).

Pellet	R_q [nm]	R_{max} [μm]
375 MPa	83 ± 42	1,07 ± 0,47
500 MPa	80 ± 28	1,26 ± 0,42

21 cycles and re-pressing at 500 MPa. The results showed a comparable structure to uncycled pellets from Fig. 10a–c with a closed surface and protruding grains. Although, considerably more larger particles >10 μm were present. Nevertheless, no trenches or pores that could significantly hinder contact with the ATR element were observed.

Despite the re-pressed samples' well-appearing optical surface characteristics, no detectable spectral changes could be recorded via the FTIR-ATR setup. A more detailed look at the samples revealed that the pellet surface appears microscopically smooth but becomes uneven in the overall texture. The effect may be illustrated by the behavior of a pellet like a spring during re-compaction. In this case, a pellet is tensioned elastically when the compaction pressure is applied, and not only plastically, like one would prefer (cf. [20]). When the pressure is released, this may lead to a relaxation of the material, which manifests in a surface of high unevenness or waviness. This, in turn, does not allow sufficient contact with the ATR element. Similarly, a local swelling during cycling can lead to a wavy surface and geometric deformation. Another drawback arises from the easy damage or breakage of a pellet during insertion or removal from the press die. Moreover, the method is quite inconvenient, as the pellet would have to be (regularly) removed to smooth the surface, e.g., for the use in a filling-level sensor.

The results showed that the surface roughness needs to be considered at different length scales (see Fig. 12a). Roughness measured by SFM represents the surface variation in-depth and height of peaks and notches on a microscopic scale, i.e., a lateral scale up to 100 μm. Waviness, describes surface irregularities on a macroscopic scale, i.e., millimeters to centimeters. Concerning the ATR measurement, microscopic and macroscopic length scales can play a role. For a wavy sample, only partial contact with the ATR element can be established (Fig. 12b). Then at this scale, also the microscopic roughness plays a role as the ATR signal can only be obtained at the contact areas. The presence of a significant waviness and structural deformation can already be seen by the optical reflections of the pellet surface, especially for the sample after 28 cycles (Fig. 7). Therefore, the results suggest that waviness in the sample surface is the dominating factor. This also agrees with the previously shown observations for samples after 30 cycles (Fig. 8), as their roughness was determined in a comparable range regardless of treatment.

To reduce the influence of sample waviness, adjusting the pellet geometry was followed. A thin pellet (<1 mm) is less resistant to bending and should better attach to the ATR surface. However, thickness deviations in the range of ±0.2 mm were found for thin pellets using a thickness gauge, which counteracted a sufficient optical contact. Besides, Pohlmann et al. [20] reported that the formation of pellets with a thickness below 1.5 mm was not feasible due to structural integrity. Therefore, unlike the handling equipment used, a more advanced preparation technique is a prerequisite to achieve a uniform powder distribution in the press die for the

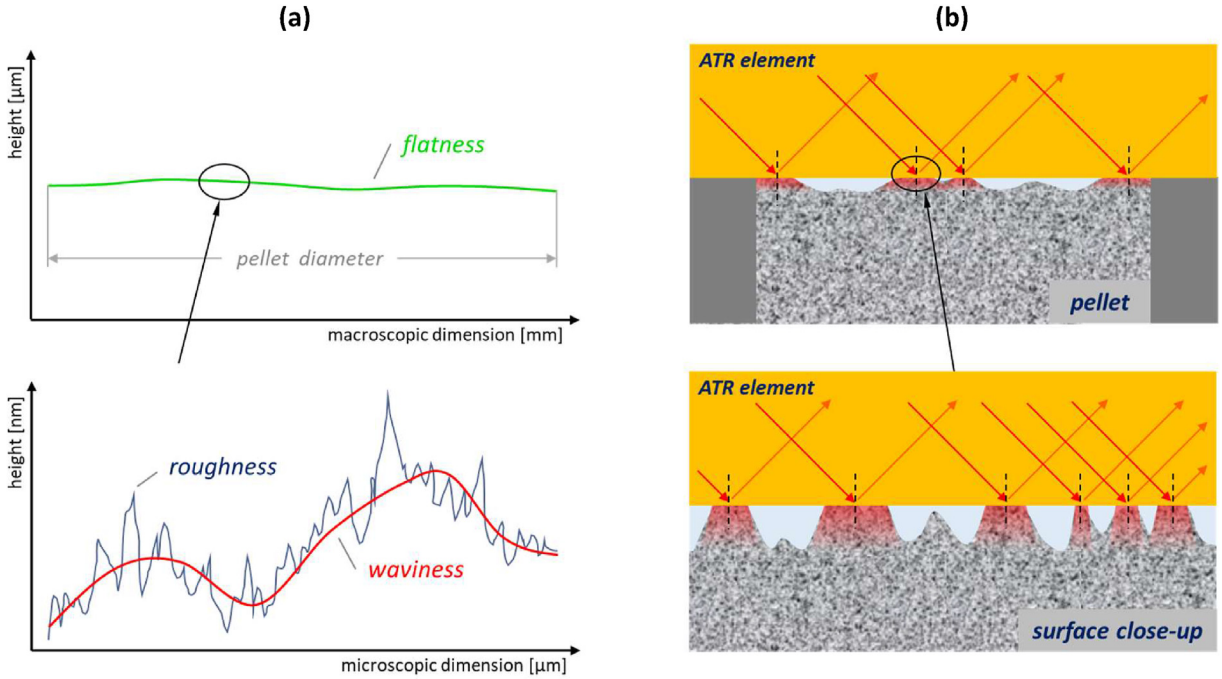

Fig. 12 – a) Schematic representation of macroscopic sample flatness vs. microscopic surface roughness and waviness. b) Associated contacting of a pellet to the ATR element with a close-up of the sample surface.

compaction of thin pellets with high uniformity in thickness. Another option to improve optical contact may be using smaller pellet diameters to reduce the influence of waviness due to a decreased surface area. Moreover, small diameters lead to a higher contact pressure at constant contact force. Pressing a compact ATR element into the sample, as has already been tested with a fiber-bound probe from *ArtPhotonics* [52], can also be a feasible approach to reduce the contact area. At the same time, it is crucial to ensure a reasonably large recording area to average over a large number of particles.

The obtained findings were considered for applying the ATR method for filling level detection in a metal hydride tank system. For this purpose, the pellet geometry was reduced to a diameter of 5 mm to achieve a more uniform and stable contacting. More than 50 cycles could be run through within a sensor prototype without noticeable signal degradation. A detailed presentation of the filling level sensor will be given in future work. However, at this point, a design aspect of the ATR cuvettes used should be discussed, which was implemented differently on the sensor prototype. The pellet inside the ATR cuvette is in a separate gas room to the contact spring, subjected to ambient pressure (also see Fig. 1 and Ref. [38]). Therefore, the contact spring has to work against the internal pressure of the cuvette. As a result, an alternating contact pressure occurs with the ab-/desorption steps passed through. In contrast, the sample and contact spring of the sensor prototype are located in the same gas room, which means that the contacting is not affected by pressure changes. Consequently, a more uniform and constant contacting is realized, providing a more stable optical data acquisition for long-term monitoring.

Conclusion

The hydrogen desorption behavior of $TiCl_3$-doped $NaAlH_4$ compacts at elevated cycle numbers (>10) was investigated by a parallel FTIR-ATR spectroscopic and gravimetric measurement method with a cycling setup for hydrogen ab-/desorption. An optical signal degradation and even a complete signal loss became apparent during cycling. Temperature changes between operating conditions (>100 °C) and non-operating conditions (room temperature) of the alanate material were identified to promote the optical signal degradation. Although neither loss of structural integrity nor decrepitation or disaggregation of the pellets occurred within 30 cycles, changes in the pellets' surface morphology were evident by visual inspection. Using SEM and SFM measurements, a surface roughening and pore formation induced by cycling was found. Thereby, the resulting poor contact between the sample and the ATR element can lead to optical signal degradation.

Through various approaches to ensure reliable optical signal detection, it was found that dimensional changes in the surface flatness of the pellets play a dominant role compared to the surface roughness. When signal quality is poor, attempts are usually made to increase the contact area for the ATR method, e.g., using a multi-bounce ATR unit. Here in turn, the findings suggest that the contact area should be reduced, since the influence of flatness increases with surface area. This follows from the fact that $NaAlH_4$ represents a strong absorber and the achieved signal-to-noise ratios through single reflection are of reasonable quality. Consequently, multiple reflections would further reduce the signal quality due to the strong absorption and thus low signal strength. A reduced contact area can be achieved by using small pellet diameters ($\varnothing \approx 5$ mm) or partially contacted sample areas. Furthermore, the observations indicated that for a more durable signal acquisition an alternating contact force, as occurs within the ATR cuvettes, should be circumvented. This can be achieved by setting up the contacting device and sample in the same gas room when alternating gas pressures are necessary for sorption mechanisms. Of course, the measures described are not limited to the studies applied and can be implemented to other materials (in-/excluding sorption processes) or similar measurement methods.

Due to the remaining potential of long-term signal degradation, future investigations by means of surface profilometry or similar measuring methods should be used to capture the overall surface characteristics, especially in terms of flatness/waviness. Moreover, it needs to be clarified how far a varying elemental surface composition can affect the optical signal (e.g., an enhanced Al concentration on the particle surface, cf. [40]). To enhance the optical contact, a further viable route could be high-energy ball milling during synthesis to obtain powder material in the nanometer range. This can result in a more homogeneous pellet formation with highly uniform surface characteristics. A similar effect might be achieved by direct thermal as well as gas sorption treatment of the material within the press die during compaction. Another concept could be the direct material deposition of $NaAlH_4$ onto the ATR element by a sputter process to create a strong interconnection between the materials.

The experiments underline that the ATR method, which is widely used in practice, requires a more sophisticated handling when accompanied by sorption mechanisms and temperature changes. Up to this point, a small contact area in the range of 1 mm^2–2.5 mm^2 with constant contact pressure seems to be the most suitable approach. Although no long-term stable signals could yet be obtained, the applied methods and findings contribute to improve the measurement procedure and to find suitable measures for permanent signal acquisition.

Declaration of competing interest

The authors declare that they have no known competing financial interests or personal relationships that could have appeared to influence the work reported in this paper.

Acknowledgment

We gratefully acknowledge the financial support from the Federal Ministry of Education and Research, HUBER+SUHNERCubeOptics AG and Anleg GmbH. Moreover, we thank H. J. Beck for the manufacturing of the cuvette components and A. Meier for the SEM measurements. In

addition, we thank C. Hess, Technical University of Darmstadt, for many helpful discussions.

Funding

Federal Ministry of Education and Research, Bundesministerium für Bildung und Forschung (ProfUnt grant no. 13FH063PX5); HUBER+SUHNER Cube OpticsAG; AnlegGmbH.

REFERENCES

[1] Staffell I, Scamman D, Velazquez Abad A, Balcombe P, Dodds PE, Ekins P, et al. The role of hydrogen and fuel cells in the global energy system. Energy Environ Sci 2019;12(2):463–91. https://doi.org/10.1039/C8EE01157E.
[2] Yue M, Lambert H, Pahon E, Roche R, Jemei S, Hissel D. Hydrogen energy systems: a critical review of technologies, applications, trends and challenges. Renew Sustain Energy Rev 2021;146(34):111180. https://doi.org/10.1016/j.rser.2021.111180.
[3] Kunowsky M, Marco-Lózar JP, Linares-Solano A. Material demands for storage technologies in a hydrogen economy. J Renew Energy 2013;2013(2823):1–16. https://doi.org/10.1155/2013/878329.
[4] Züttel A. Materials for hydrogen storage. Mater Today 2003;6(9):24–33. https://doi.org/10.1016/S1369-7021(03)00922-2.
[5] Züttel A, editor. Hydrogen as a future energy carrier. Weinheim: Wiley-VCH; 2008.
[6] Bellosta von Colbe JM, Ares J-R, Barale J, Baricco M, Buckley C, Capurso G, et al. Application of hydrides in hydrogen storage and compression: achievements, outlook and perspectives. Int J Hydrogen Energy 2019;44(15):7780–808. https://doi.org/10.1016/j.ijhydene.2019.01.104.
[7] Jepsen J, Bellosta von Colbe JM, Klassen T, Dornheim M. Economic potential of complex hydrides compared to conventional hydrogen storage systems. Int J Hydrogen Energy 2012;37(5):4204–14. https://doi.org/10.1016/j.ijhydene.2011.11.141.
[8] Ali NA, Ismail M. Modification of NaAlH4 properties using catalysts for solid-state hydrogen storage: a review. Int J Hydrogen Energy 2021;46(1):766–82. https://doi.org/10.1016/j.ijhydene.2020.10.011.
[9] Sakintuna B, Lamari-Darkrim F, Hirscher M. Metal hydride materials for solid hydrogen storage: a review. Int J Hydrogen Energy 2007;32(9):1121–40. https://doi.org/10.1016/j.ijhydene.2006.11.022.
[10] von Helmolt R, Eberle U. Fuel cell vehicles: status 2007. J Power Sources 2007;165(2):833–43. https://doi.org/10.1016/j.jpowsour.2006.12.073.
[11] Bogdanović B, Schwickardi M. Ti-doped alkali metal aluminium hydrides as potential novel reversible hydrogen storage materials. J Alloys Compd 1997;253–254:1–9. https://doi.org/10.1016/S0925-8388(96)03049-6.
[12] Bogdanovic B, Felderhoff M, Streukens G. Hydrogen storage in complex metal hydrides. J Serb Chem Soc 2009;74(2):183–96. https://doi.org/10.2298/JSC0902183B.
[13] Guerrero-Ortiz R, Tena-García JR, Flores-Jacobo A, Suárez-Alcántara K. From the can to the tank: NaAlH4 from recycled aluminum. Int J Hydrogen Energy 2019;44(36):20183–90. https://doi.org/10.1016/j.ijhydene.2019.06.033.
[14] Bergemann N, Pistidda C, Milanese C, Girella A, Hansen BRS, Wurr J, et al. NaAlH4 production from waste aluminum by reactive ball milling. Int J Hydrogen Energy 2014;39(18):9877–82. https://doi.org/10.1016/j.ijhydene.2014.02.025.
[15] Sandrock G, Gross K, Thomas G. Effect of Ti-catalyst content on the reversible hydrogen storage properties of the sodium alanates. J Alloys Compd 2002;339(1–2):299–308. https://doi.org/10.1016/S0925-8388(01)02014-X.
[16] Anton DL. Hydrogen desorption kinetics in transition metal modified NaAlH4. J Alloys Compd 2003;356–357:400–4. https://doi.org/10.1016/S0925-8388(03)00140-3.
[17] Bogdanović B, Felderhoff M, Pommerin A, Schüth F, Spielkamp N. Advanced hydrogen-storage materials based on Sc-, Ce-, and Pr-doped NaAlH4. Adv Mater 2006;18(9):1198–201. https://doi.org/10.1002/adma.200501367.
[18] Wang T, Wang J, Ebner AD, Ritter JA. Reversible hydrogen storage properties of NaAlH4 catalyzed with scandium. J Alloys Compd 2008;450(1–2):293–300. https://doi.org/10.1016/j.jallcom.2006.10.072.
[19] Kim KJ, Montoya B, Razani A, Lee K-H. Metal hydride compacts of improved thermal conductivity. Int J Hydrogen Energy 2001;26(6):609–13. https://doi.org/10.1016/S0360-3199(00)00115-4.
[20] Pohlmann C, Röntzsch L, Hu J, Weißgärber T, Kieback B, Fichtner M. Tailored heat transfer characteristics of pelletized LiNH2–MgH2 and NaAlH4 hydrogen storage materials. J Power Sources 2012;205:173–9. https://doi.org/10.1016/j.jpowsour.2012.01.064.
[21] Lozano GA, Ranong CN, Bellosta von Colbe JM, Bormann R, Hapke J, Fieg G, et al. Optimization of hydrogen storage tubular tanks based on light weight hydrides. Int J Hydrogen Energy 2012;37(3):2825–34. https://doi.org/10.1016/j.ijhydene.2011.03.043.
[22] Khalil YF, Opalka SM, Laube BL. Experimental and theoretical investigations for mitigating NaAlH4 reactivity risks during postulated accident scenarios involving exposure to air or water. Process Saf Environ Protect 2013;91(6):463–75. https://doi.org/10.1016/j.psep.2012.10.013.
[23] Lozano GA, Bellosta von Colbe JM, Bormann R, Klassen T, Dornheim M. Enhanced volumetric hydrogen density in sodium alanate by compaction. J Power Sources 2011;196(22):9254–9. https://doi.org/10.1016/j.jpowsour.2011.07.053.
[24] Franke I, Flick T, Bauer H-D, Scheppat B. Hydrogen desorption kinetics of CeCl3-doped sodium aluminum hydride compacts measured by parallel in situ FTIR-ATR-spectroscopy and gravimetry. Int J Hydrogen Energy 2015;40(11):4175–83. https://doi.org/10.1016/j.ijhydene.2015.01.108.
[25] Franke I, Hentschel O, Nitsche D, Stops M, Bauer H-D, Scheppat B. Parallel FTIR-ATR and gravimetrical in-situ measurements on sodium alanate powder samples during hydrogen desorption. Int J Hydrogen Energy 2013;38(36):16161–7. https://doi.org/10.1016/j.ijhydene.2013.09.039.
[26] Harrick NJ. Internal reflection spectroscopy. 3rd ed. New York NY u.a.: Interscience Publ; 1967.
[27] Mirabella FM, editor. Modern techniques in applied molecular spectroscopy. New York: Wiley; 1998.
[28] Srinivasan SS, Brinks HW, Hauback BC, Sun D, Jensen CM. Long term cycling behavior of titanium doped NaAlH4 prepared through solvent mediated milling of NaH and Al with titanium dopant precursors. J Alloys Compd 2004;377(1–2):283–9. https://doi.org/10.1016/j.jallcom.2004.01.044.
[29] Lozano GA, Ranong CN, Bellosta von Colbe JM, Bormann R, Fieg G, Hapke J, et al. Empirical kinetic model of sodium alanate reacting system (I). Hydrogen absorption. Int J Hydrogen Energy 2010;35(13):6763–72. https://doi.org/10.1016/j.ijhydene.2010.04.080.

[30] Lozano GA, Ranong CN, Bellosta von Colbe JM, Bormann R, Fieg G, Hapke J, et al. Empirical kinetic model of sodium alanate reacting system (II). Hydrogen desorption. Int J Hydrogen Energy 2010;35(14):7539–46. https://doi.org/10.1016/j.ijhydene.2010.04.142.
[31] Lozano GA, Eigen N, Keller C, Dornheim M, Bormann R. Effects of heat transfer on the sorption kinetics of complex hydride reacting systems. Int J Hydrogen Energy 2009;34(4):1896–903. https://doi.org/10.1016/j.ijhydene.2008.12.028.
[32] Fan X, Xiao X, Chen L, Han L, Li S, Ge H, et al. Thermodynamics, kinetics, and modeling investigation on the dehydrogenation of CeAl 4 -doped NaAlH 4 hydrogen storage. Mater J Phys Chem C 2011;115(45):22680–7. https://doi.org/10.1021/jp208576v.
[33] Khan J, Jain IP. Chloride catalytic effect on hydrogen desorption in NaAlH4. Int J Hydrogen Energy 2016;41(19):8271–6. https://doi.org/10.1016/j.ijhydene.2015.11.116.
[34] Rafi-ud-din, Xuanhui Q, Zahid GH, Asghar Z, Shahzad M, Iqbal M, et al. Improved hydrogen storage performances of MgH2–NaAlH4 system catalyzed by TiO2 nanoparticles. J Alloys Compd 2014;604:317–24. https://doi.org/10.1016/j.jallcom.2014.03.150.
[35] Schmidt T, Röntzsch L. Reversible hydrogen storage in Ti–Zr-codoped NaAlH4 under realistic operation conditions. J Alloys Compd 2010;496(1–2):L38–40. https://doi.org/10.1016/j.jallcom.2010.02.162.
[36] Schmidt T, Röntzsch L, Weißgärber T, Kieback B. Influence of transition metal dopants and temperature on the dehydrogenation and rehydrogenation kinetics of NaAlH4. Int J Hydrogen Energy 2012;37(5):4194–200. https://doi.org/10.1016/j.ijhydene.2011.11.139.
[37] Sulic M, Cai M, Kumar S. Cycling and engineering properties of highly compacted sodium alanate pellets. Int J Hydrogen Energy 2012;37(20):15187–95. https://doi.org/10.1016/j.ijhydene.2012.07.113.
[38] Enders M, Kleber M, Derscheid G, Hofmann K, Bauer H-D, Scheppat B. Parallel FTIR-ATR spectroscopy and gravimetry for the in situ hydrogen desorption measurement of NaAlH4 powder compacts. Appl Opt 2020;59(30):9510–9. https://doi.org/10.1364/AO.403846.
[39] Berger R, Domanski AL, Weber SAL. Electrical characterization of organic solar cell materials based on scanning force microscopy. Eur Polym J 2013;49(8):1907–15. https://doi.org/10.1016/j.eurpolymj.2013.03.005.
[40] Thomas GJ, Gross KJ, Yang NYC, Jensen C. Microstructural characterization of catalyzed NaAlH4. J Alloys Compd 2002;330–332:702–7. https://doi.org/10.1016/S0925-8388(01)01538-9.
[41] Gomes S, Renaudin G, Hagemann H, Yvon K, Sulic MP, Jensen CM. Effects of milling, doping and cycling of NaAlH4 studied by vibrational spectroscopy and X-ray diffraction. J Alloys Compd 2005;390(1–2):305–13. https://doi.org/10.1016/j.jallcom.2004.08.036.
[42] Parker SF. Spectroscopy and bonding in ternary metal hydride complexes—potential hydrogen storage media. Coord Chem Rev 2010;254(3–4):215–34. https://doi.org/10.1016/j.ccr.2009.06.016.
[43] Wang X, Andrews L. Sodium hydride clusters in solid hydrogen and neon: infrared spectra and theoretical calculations. J Phys Chem A 2007;111(30):7098–104. https://doi.org/10.1021/jp0727852.
[44] Filippi M, Rector JH, Gremaud R, van Setten MJ, Dam B. Lightweight sodium alanate thin films grown by reactive sputtering. Appl Phys Lett 2009;95(12):121904. https://doi.org/10.1063/1.3236525.
[45] Pohlmann C, Röntzsch L, Kalinichenka S, Hutsch T, Kieback B. Magnesium alloy-graphite composites with tailored heat conduction properties for hydrogen storage applications. Int J Hydrogen Energy 2010;35(23):12829–36. https://doi.org/10.1016/j.ijhydene.2010.08.104.
[46] Pohlmann C, Röntzsch L, Kalinichenka S, Hutsch T, Weißgärber T, Kieback B. Hydrogen storage properties of compacts of melt-spun Mg90Ni10 flakes and expanded natural graphite. J Alloys Compd 2011;509:S625–8. https://doi.org/10.1016/j.jallcom.2010.11.060.
[47] Börries S, Metz O, Pranzas PK, Bellosta von Colbe JM, Bücherl T, Dornheim M, et al. Optimization and comprehensive characterization of metal hydride based hydrogen storage systems using in-situ Neutron Radiography. J Power Sources 2016;328(7):567–77. https://doi.org/10.1016/j.jpowsour.2016.08.040.
[48] van Hassel BA, Mosher D, Pasini JM, Gorbounov M, Holowczak J, Tang X, et al. Engineering improvement of NaAlH4 system. Int J Hydrogen Energy 2012;37(3):2756–66. https://doi.org/10.1016/j.ijhydene.2011.02.005.
[49] Dieterich M, Pohlmann C, Bürger I, Linder M, Röntzsch L. Long-term cycle stability of metal hydride-graphite composites. Int J Hydrogen Energy 2015;40(46):16375–82. https://doi.org/10.1016/j.ijhydene.2015.09.013.
[50] Jepsen J, Milanese C, Girella A, Lozano GA, Pistidda C, Bellosta von Colbe JM, et al. Compaction pressure influence on material properties and sorption behaviour of LiBH4–MgH2 composite. Int J Hydrogen Energy 2013;38(20):8357–66. https://doi.org/10.1016/j.ijhydene.2013.04.090.
[51] Sulic M, Cai M, Kumar S. Controlled degradation of highly compacted sodium alanate pellets. Int J Hydrogen Energy 2013;38(7):3019–23. https://doi.org/10.1016/j.ijhydene.2012.12.093.
[52] Art photonics. Fiber optics company | photonics solutions | fiber solutions. 2021. Available from: https://artphotonics.com/.